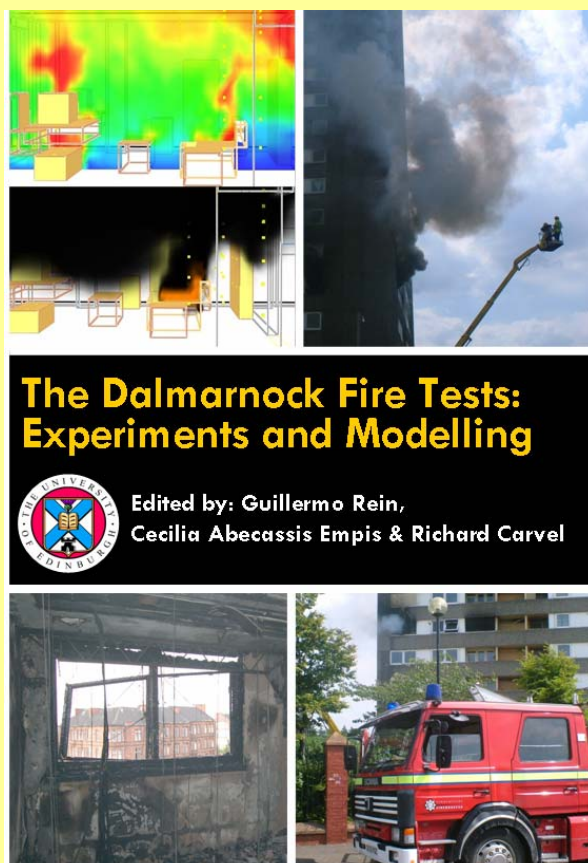*This PDF file is an extract from:*

The Dalmarnock Fire Tests: Experiments and Modelling
Edited by G. Rein, C. Abecassis Empis and R. Carvel

Published by the School of Engineering and Electronics, University of Edinburgh, 2007.
ISBN 978-0-9557497-0-4

The contents of the book and much of the other published output from the BRE Centre for Fire Safety Engineering can be downloaded for free from the Edinburgh Research Archive:
http://www.era.lib.ed.ac.uk/handle/1842/1152

Produced as part of the FIRESEAT symposium series:
http://www.fireseat.org/

3. Test One: The 'Uncontrolled' Fire

By Cecilia Abecassis Empis, Adam Cowlard,
Stephen Welch & José L. Torero

Introduction

The first of the Dalmarnock Fire Tests was a post-flashover compartment fire experiment held on July 25th, 2006, in a two-bedroom single-family flat on the 4th floor of the 23-storey reinforced concrete tower in Dalmarnock, Glasgow, where the tests were held. The main experimental compartment was a fully-furnished living room/office space, instrumented with a high density of fire- and structural-monitoring sensors where a fire was allowed to develop freely to post-flashover conditions. A detailed description of the set-up of this test, including compartment layout, fuel and ventilation conditions and specifics of the monitoring sensors can be found in Chapter 2. Major events throughout the 19 min fire are reported followed by a thorough characterisation of the fire using sensor information. The characterisation of Test One provides a platform with potential for analytical and computational fire model validation.

Major Events

The experimental compartment was stripped and fitted with furniture and sensors during the days prior to the test however ventilation parameter arrangements and final data logger checks were only made just prior to ignition on the test day. Cameras placed with several view points within the compartment provide a visual record of some of the key events in the fire.

Prior to ignition, data logging was commenced to record ambient conditions. 500ml of heptane (accelerant) was poured into the waste-paper basket, soaking some of the crumpled up newspaper within it. At 12:23:00 a blow torch was used to pilot ignition of the contents of the wastepaper basket and the fire was allowed to grow unconstrained. A blanket draped over the sofa arm, dangling over the wastepaper basket, caught fire almost immediately. In turn, this ignited several cushions with fire spreading swiftly to engulf the polyurethane sofa. Four and a half minutes of sofa burning led to ignition of the contents of the bookcase adjacent to the sofa and waste-paper basket, close to the NE corner of the room. Fire progressed up the bookcase followed by a flashover period which saw ceiling flame projection into the Flat Corridor, sudden reduced visibility in the main 4th floor corridor and simultaneous ignition of paper items in several locations (Figure 1). This was swiftly followed by rapid descent of the smoke layer to floor level.
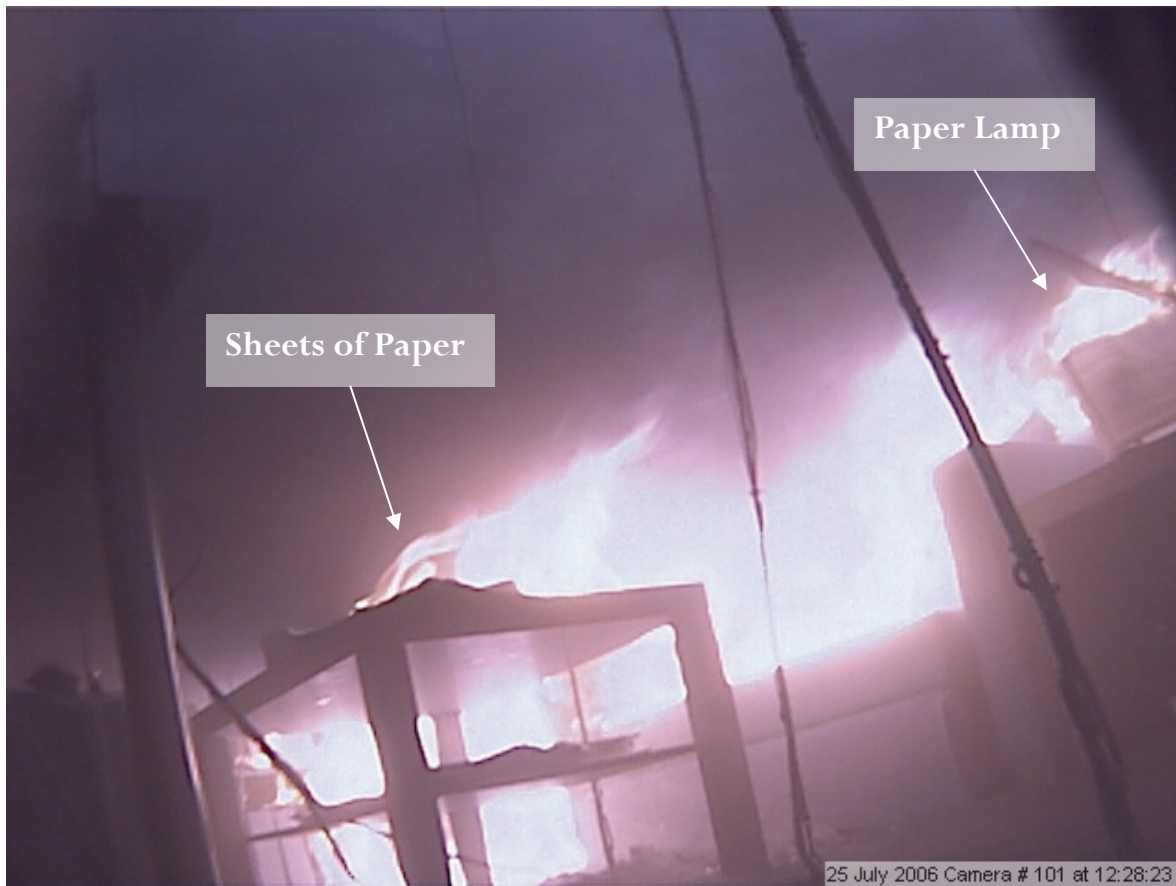
Figure 1. Camera footage of simultaneous ignition of paper items in several locations throughout the compartment at 12:28:23, indicative of the flashover period.

Consequently, post-flashover the visibility in the compartment was drastically reduced, so camera footage provides little information about the subsequent progression of fire spread. Nevertheless, analysis of the fire sensor data shows the fire burnt steadily for the next eight minutes and black smoke was externally observed seeping out around the compartment window which was not completely sealed or made air tight. The kitchen window was observed to shatter around seven minutes after the onset of flashover, even though it had been left partially open, but the experimental compartment window remained intact. The compartment's north-west (NW) window pane was broken manually 13 min 21 s into the fire. For a while mostly dark smoke was seen billowing out with sustained external flaming developing four and a half minutes later. Moments after this the second window pane shattered. The fire was allowed to burn freely for a total of 19 min before the fire brigade intervened to extinguish the fire. A summary of the time to key events is provided in Table 1.

Major Events Observed	Time (h:m:s)	Time from Ignition (s)
Growth Period		
Ignition	12:23:00	0
Cushions ignite	12:23:09	9
Smoke visible in main corridor	12:26:06	186
Bookcase ignites	12:27:35	275
Flashover Period		
Fire engulfs bookcase	12:28:00	300
Flames project to Flat Corridor ceiling, low visibility in main corridor	12:28:15	315
Ignition of paper lamp and paper on table	12:28:23	323
Post-Flashover Period		
Kitchen Window breakage	12:35:00	720
Compartment window breakage (NW Pane)	12:36:21	801
External flaming	12:41:00	1080
Compartment window breakage (SW Pane)	12:41:31	1111
Firemen in, begin to extinguish	12:42:00	1140
Mostly Smouldering	12:45:00	1320

Table 1. List of major events observed in camera footage throughout the 'uncontrolled' fire (Test One) and respective clock time and time elapsed from ignition.
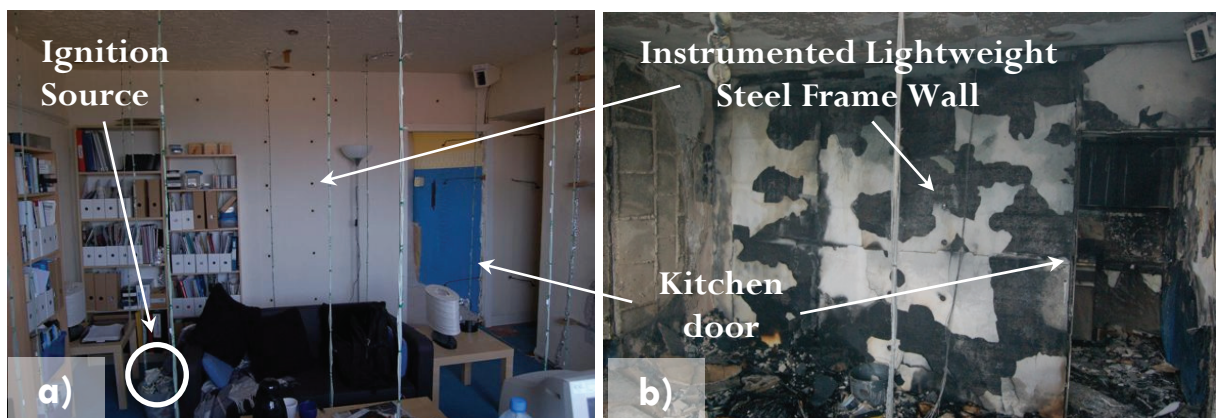

Figure 2. View of the ignition source, sofa, bookcases and nearby items in the experimental compartment both, a) before the fire, and b) after the fire.

A survey of the aftermath showed only a few metal components and some charred paper remained unconsumed while most of the experimental compartment fuel had burnt out (Figure 2.) Fortunately all thermocouple trees were still found to be in place, hence original thermocouple coordinates logged are assumed to hold true for all thermocouple data recorded throughout the test.

Data Processing

Sensor Calibration

Laboratory calibration of most sensors used in the test was conducted as required for data post-processing. Laboratory calibration of the laser obscuration sensors allowed for conversion of the raw voltage data obtained into the form of relative power and as such, percentage obscuration. In turn this enabled calculation of an average extinction coefficient of the smoke layer, allowing for thermocouple temperature data to be corrected for gas-phase temperature readings. Thermocouple cable used was also tested at BRE against calibrated thermocouple blocks to determine any errors involved in its reading of temperature. Experimental heat flux gauges, in the form of thin-skin calorimeters, were calibrated using an attuned Heat Flux Meter and a radiative panel, such that temperatures recorded could be converted to an equivalent net incident heat flux. Conversion of the raw data from the Bi-directional Velocity Probes was performed as per literature detailing the calibration of such probes in a wind tunnel at BRE (*cf.* McCaffrey *et al*. 1976, Welch *et al*. 2007). Details of the calibration process of most sensor types can be found in Chapter 2. Camera footage, which was also streamed live to a control room during the event, required no post-processing.

Smoke Layer

Thermocouple temperature measurements were used to determine the height of the smoke layer over time. This 'height' indicates the distance from the floor to the boundary between the hot smoke layer above and the cooler air underneath. The conversion of the field measurements to zone-type data was done assuming that the smoke layer interface is located near the 100°C isotherm (averaged height throughout compartment). This data-derived smoke layer height was verified against visual estimates from camera footage, where the smoke layer height was taken when a visible, sustained boundary layer reached the height of known objects. Camera footage provides only a crude estimate of the smoke layer height due to turbulent flows often creating a slightly indistinct boundary layer between the evidently smoke-filled and non smoke-filled areas. While thermocouple-derived smoke layer height is overall more dependable, it is also constrained by limitations such as the density of thermocouple measurement points. Hence camera footage is useful in verifying the overall trend of the smoke layer height variation in time and becomes particularly useful in establishing the initial height of the smoke layer (*i.e.* at ignition) before it descends to the uppermost thermocouple used in the smoke layer

height calculation (*i.e.* at 2400mm height). Similarly, camera footage is used to determine the smoke layer height once the layer has grown beyond the lowermost thermocouple (*i.e.* at 450mm height) by following the trend observed once the thermocouple-derived data began to stabilise. The variation in smoke layer height (Figure 3) is required for use in determining the equivalent extinction coefficient of the smoke layer.
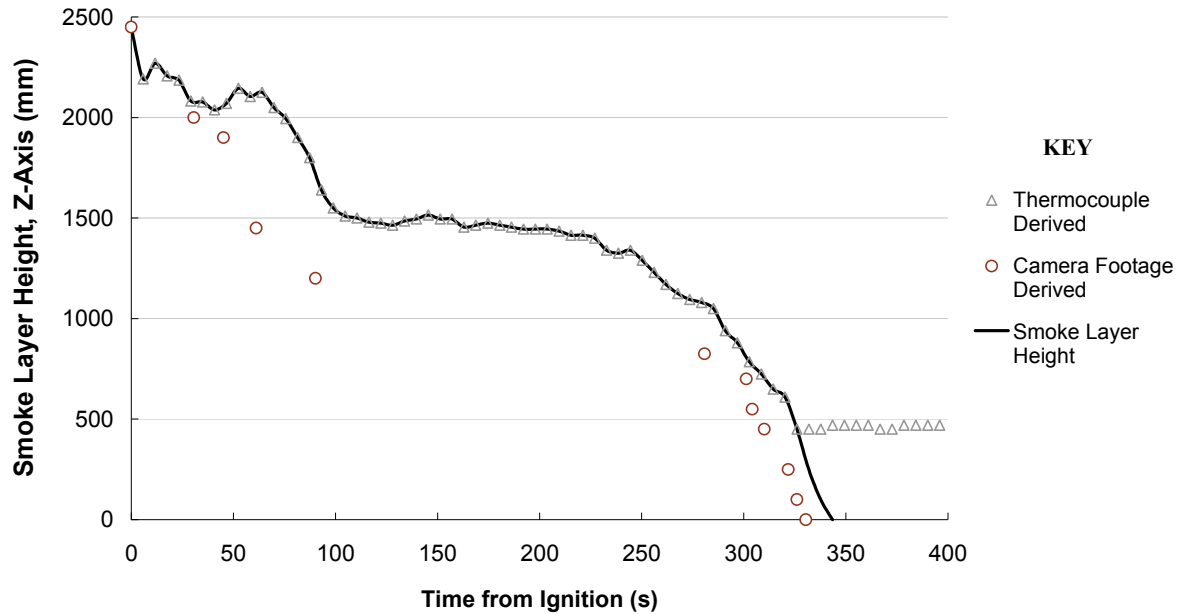

Figure 3. Height of the Smoke Layer within the experimental compartment, derived from a combination of thermocouple data and camera footage.

Extinction Coefficients

An extinction coefficient of the smoke layer was established using post-processed laser data in the form of relative power, following the classical methodology based on Bourger's Law (Mulholland 2002), described in detail in Chapter 2. Contrary to expectation, it was found that the vertically aligned laser pairs yielded extinction coefficients noticeably lower than the lasers mounted on the wall. There was also a clear correlation between the location of vertical lasers yielding lower extinction coefficients and regions of known flaming. It was concluded that, although the optical filter used over the receiver was adequate for screening out background visible light out with the small bandwidth of the laser emitter, it did not filter out all wavelengths in the infrared region. Since in all three cases the vertical laser receiver was located at floor level, the smoke layer did not obstruct the infrared radiation emitted by the flames from impinging directly on the laser receiver until it had grown to significant depth. This explains why the vertical laser data registered relatively high voltages when camera footage shows the concurrent smoke layer already had considerable density and depth and is confirmed by the sudden rise in extinction coefficient resulting from this laser data about 330 s into the fire, when the smoke layer descended to floor level. Hence percentage obscuration information obtained from the vertical laser pairs has been deemed inaccurate.

Additionally, just after the onset of flashover all the laser data began to fluctuate erratically, most likely due to heat damage, and therefore is only considered reliable up to this point. Nevertheless, camera footage from a camera stationed on the wall opposite the horizontal lasers, at a height of 730 mm off the floor, was used for simple verification of the extinction coefficient calculations. Jin has stated that once a light-reflecting object is visually judged to be "*just* no longer visible" due to smoke obscuration, the extinction coefficient of the smoke layer at that time is the quotient of three over the distance to that object (Mulholland 2002, Jin 2002). Hence, the distance to referenced objects in the horizontal line of sight of the footage was estimated from plan drawings of the furnished compartment and used to populate this correlation. The data was found to have good correspondence with the laser-obtained extinction coefficients, inclusive of a data point within the flashover period as is evident in Figure 4. In particular it was seen to correspond to the data obtain from the lowest set of horizontal lasers (Laser 1), which was located at a similar height to the camera recording footage used.
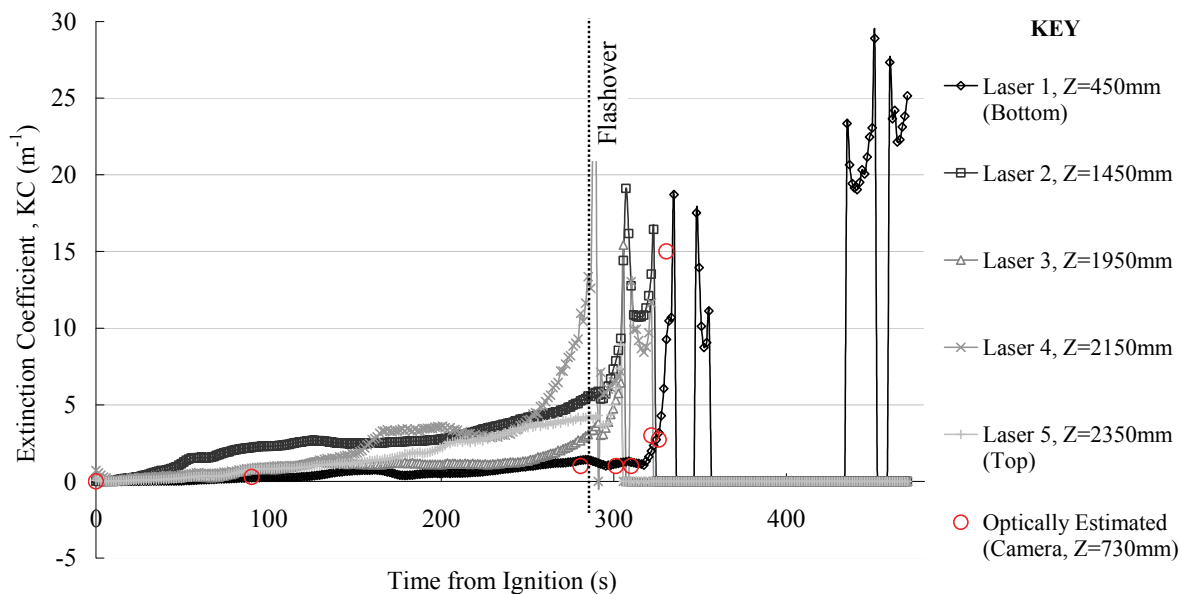

Figure 4. Extinction Coefficient data calculated from each horizontal laser measurement of smoke obscuration, together with optically estimated extinction coefficient of the smoke layer for comparison.

The various measurements taken enabled a characteristic pre-flashover extinction coefficient of the smoke layer to be calculated by averaging the extinction coefficients of only data from laser sensors submerged in the smoke layer as it descended, in time. The camera verified steep increase in extinction coefficient, around the onset of flashover seen in Figure 4, allows for the trend to be extrapolated post-flashover since evidence from footage also shows that shortly after 300 s into the fire the smoke layer descended to the ground. The lowest set of horizontal lasers (Laser 1) also output some data around 440-470 s that could be seen to fit this trend. Although its location is thought to have allowed this set of laser sensors to have remained functional for longer than the others, the reliability of this information is uncertain, not only because it appears to previously falter but also because high extinction coefficients equate to very low voltage and any errors are

therefore a larger percentage of the weaker signal. Therefore a range of bounds have been assumed for the extinction coefficient beyond flashover. Since the fire quickly became ventilation controlled, for the extrapolation it is assumed the extinction coefficients stabilised fairly quickly. The upper bound stabilisation value estimated was an extinction coefficient of 25 m^{-1}, taking into account the last set of data output by Laser 1. The lower bound stabilisation value was taken at an extinction coefficient of 14 m^{-1} since this was the last value computed from many of the sensors' output before they became damaged. For the average extinction coefficient of the smoke layer post-flashover, a gradual increase towards a stabilisation value of 19.5 m^{-1} was assumed as a mean of the estimated bounds.

While it is appreciated that the lasers were only measuring smoke obscuration in one location and that the smoke density is likely to have been spatially varied, particularly since the measurements were taken next to a wall, it is also deemed unlikely to have varied significantly given the dimensions of the compartment and its ventilation conditions. Therefore, throughout the compartment, it was assumed that the extinction coefficient had only a vertical variation, which was in any case relatively small and hence averaged out as a single value for the smoke layer as it descended over time.

Thermocouple-Temperature Correction to Gas-Phase Temperature

The thermocouple data recorded was corrected for radiation according to the method described by Welch *et al.* (2007). All thermocouples were corrected with the exception of the uppermost thermocouple in each of the 20 trees. Since these thermocouples were in contact with the ceiling their readings did not lend themselves to correction for 'gas-phase' temperature.

For evaluation of the sensitivity of the temperature correction to the range of extinction coefficients established, the correction was conducted threefold: once using the average smoke layer extinction coefficient variation over time, another using the upper-bound extinction coefficient variation and the third using the lower-bound values. The importance of the degree of accuracy of the extinction coefficient was assessed by means of comparison of the single *maximum* required temperature correction (as a difference between thermocouple-temperature and corrected gas-phase temperature) and of the *average* degree of maximum temperature correction required to each thermocouple, in each of the three cases. The comparison showed the range of extinction coefficients within the considered bounds to have a negligible difference. The maximum difference in *maximum* temperature correction to each thermocouple within the bounds (difference between upper- and lower-bound solution), was of the order of ±18°C and the maximum difference in the average correction to all thermocouple measurements taken in time was of the order of ±1°C. Hence thermocouple-temperature corrections using the average extinction coefficient were used for further comparison with raw thermocouple-temperatures.

Comparison of the thermocouple-temperature with the temperatures corrected for gas-phase revealed radiation errors to be overall negligible, since the average of the *maximum*

temperature correction per thermocouple was of the order of $\pm 7^{\circ}$C and the average global temperature correction for all thermocouples at all measurements taken in time was $\pm 0.09\,^{\circ}$C. Some localised corrections were of greater significance, such as the single maximum correction of 80°C to one thermocouple for a single measurement in time, occurring during the period of greatest temperature stratification, particularly when the hot layer initially developed. It was noticed that most temperature corrections of similar magnitude coincided in time and corresponded to thermocouples in the vicinity of the sofa and the central coffee table, as would be expected. Nevertheless the overall corrections due to radiation were relatively low compared to *average* compartment temperatures which ranged from 23°C to 990°C, especially when considering other errors involved in thermocouple measurements themselves (accurate to $\pm 5^{\circ}$C at maximum temperatures monitored) and in measurement and calculation of other parameters involved in the correction procedure.

Nevertheless, corrected gas-phase temperatures have been used throughout the analyses and this process allowed for the identification of any damaged thermocouples for which substitute values were spatially interpolated from neighbouring thermocouple readings.

Characterisation of the Fire

The nature of the Dalmarnock Fire Tests, with their dense network of sensors, have allowed for analysis of several different features of the fires, such that the characterisation of Test One comprises several different aspects of customary fire characterisation.

Six key time steps representing periods of significant change throughout the fire have been selected for comparison of different features of the fire characterisation. The time steps were chosen such that: Time Step 1 at 201s represents the initial localised sofa fire; Time Step 2 at 251s, the fire growth period as it began to spread; Time Step 3 at 351s, conditions just after flashover; Time Step 4, post-flashover steady-state conditions at 420s; Time Step 5, a period of steady temperature rise post steady-state at 661s; and, Time Step 6, at 901s, represents the period of peak average compartment temperatures once the first window pane broke. No subsequent time steps were taken as the fire was not allowed to self-extinguish.

Average Temperature-Time Curve

The compartment average gas-phase temperature-time curve provides an overview of the general fire behaviour over time. Figure 5 shows the variation in average compartment gas-phase temperature together with its standard deviation which indicates the degree of temperature heterogeneity throughout the compartment. The general behaviour of the fire seen in Figure 5 corresponds to the observed sequence of major events noted from camera footage. Key Time Steps are also indicated on Figure 5 to illustrate their significance relative to general fire behaviour.

The average temperature is seen to steadily grow for the first 100 s reaching a small period of steady-state while the sofa is burning, lasting about 100 s, point at which Time Step 1 is taken. This period represents a localised fire where overall compartment temperature standard deviation is relatively low. As the fire begins to spread, average compartment temperatures rise, leading to an overall slightly larger standard deviation in compartment temperatures as a larger proportion of thermocouples are affected by the fire and smoke. A very steep rise in average compartment temperature around 300 s into the fire is a clear indication of the flashover period observed soon after the fire spread to a fully-loaded bookcase in close proximity. At this point the compartment temperature standard deviation is at its highest, decreasing significantly as the average temperature drops to a quasi-steady state condition. This is followed by a slight, gradual rise in average temperature which sees a further decrease in standard deviation just before the first compartment window pane was broken. This change in ventilation conditions leads to a second significantly steep rise in average compartment temperatures, indicating that the fire had become ventilation-controlled in the post-flashover period leading up to this event. This is also confirmed by external video footage that showed large quantities of black smoke emanating from the compartment window once it had been broken. Around 900 s in to the fire, the average compartment temperature reaches a small quasi-steady state period at peak average temperatures, with a standard deviation similar to that during the previous period of quasi-steady state. Small variation in average temperature ensues, followed by fire brigade intervention. Camera footage of this event shows it to perfectly coincide with the timing of onset of the cooling period, evident in average compartment temperature measurements.
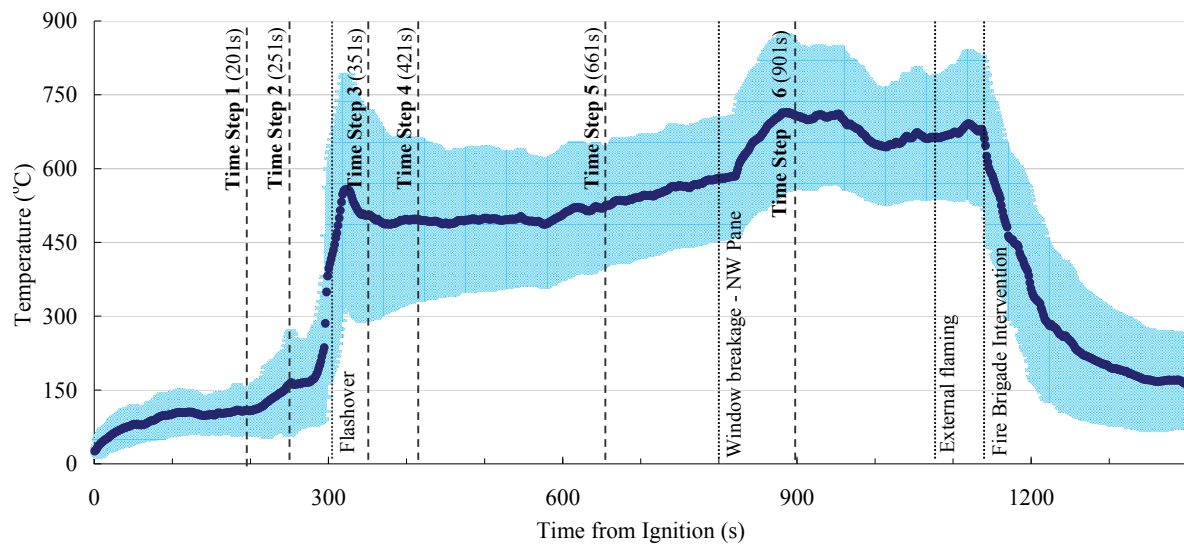

Figure 5. Gas-phase average compartment temperature-time variation with shaded region indicating the standard deviation of temperature throughout the compartment. Vertical dashed lines indicate Time Steps used for analysis and dotted lines represent time of some major events, as labelled.

Temperature Contour Plots

Two-dimensional temperature contour plots were generated through several vertical planes across the compartment in order to illustrate the spatial variation in compartment temperature throughout the development of the fire, at each of the previously defined Time Steps. Although thermocouple trees were not arranged in orthogonal lines, slice planes were taken at best-fit lines through the trees such that no tree fell outwith 0.3m of the slice plane, therefore no 3D data smoothing was required. Eleven thermocouples between the heights of 450-2400mm were used, once again excluding the uppermost thermocouples in each tree since they were in contact with the ceiling. The plots indicate the evolution of the fire as well as the spatial temperature variation.
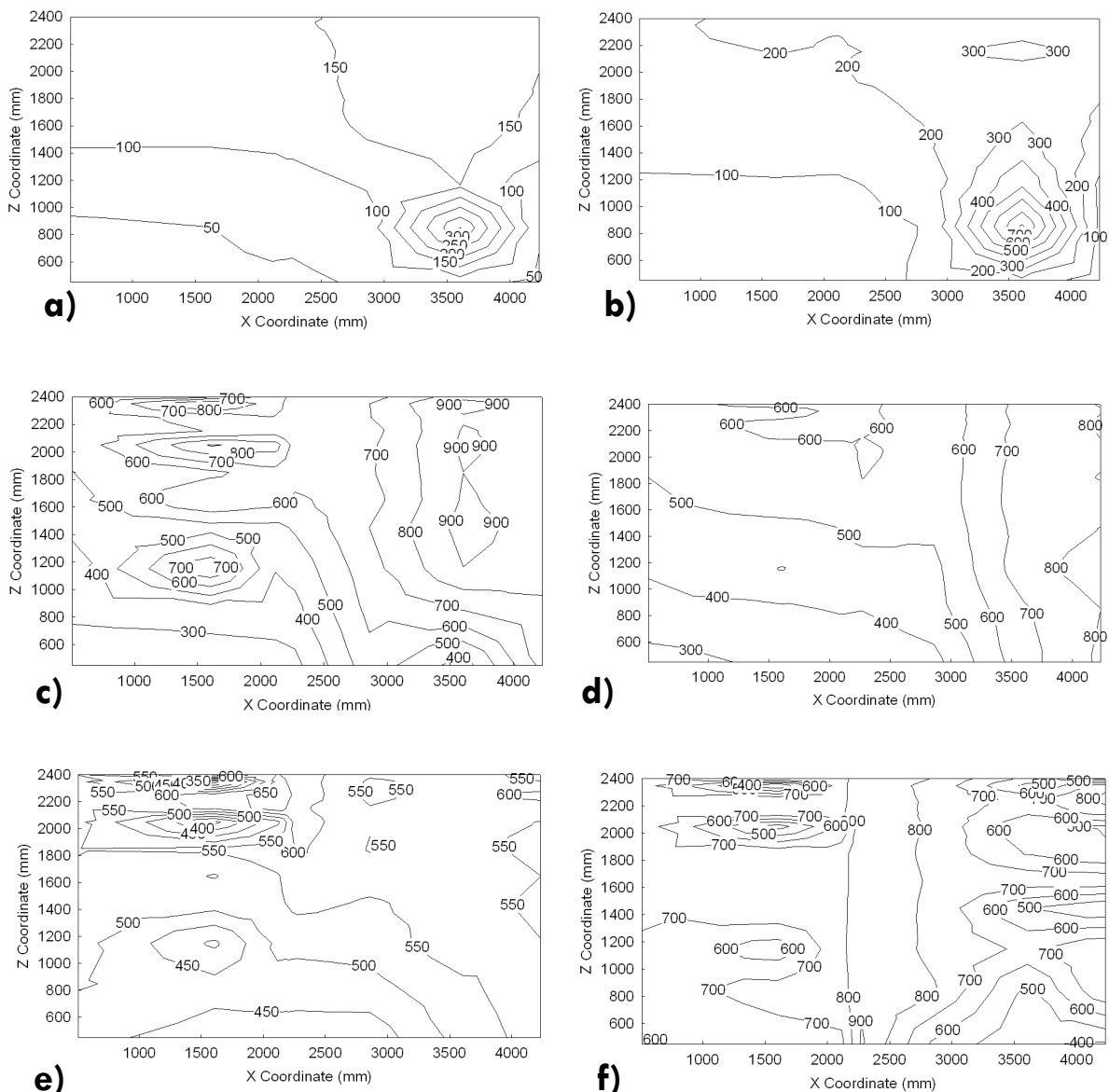

Figure 6. Gas temperature contours (in °C) taken from section S1–S1, axes values reading distances from the global origin (*cf.* Figure 7). Plots appear in the Time Step chronological order, at times from ignition: a) 201 s, b) 251 s, c) 351 s, d) 420 s, e) 661 s, and f) 901 s.
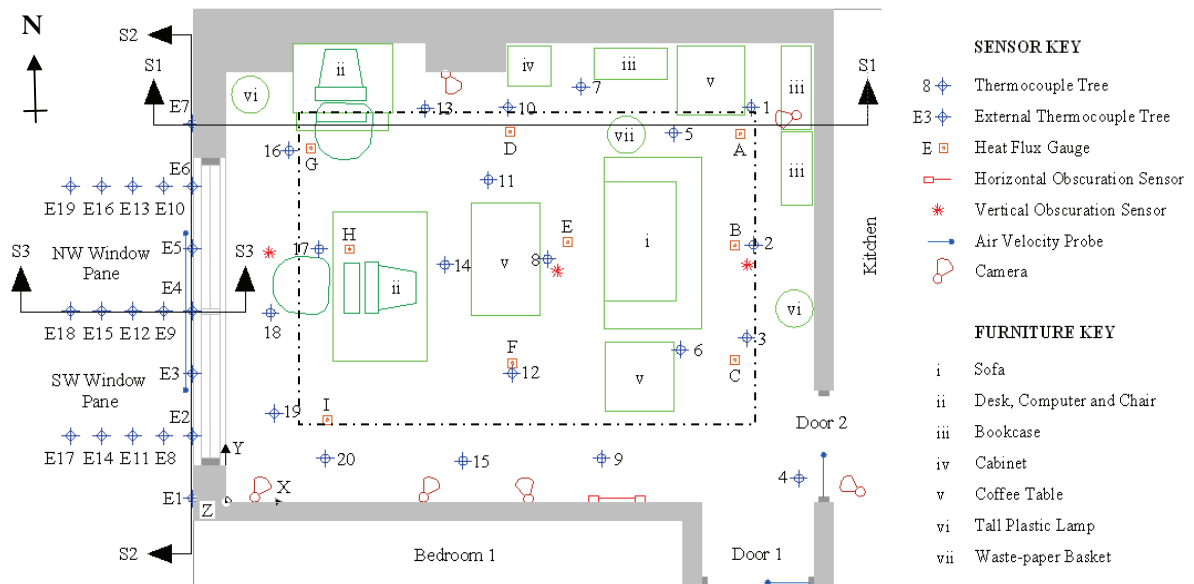
Figure 7. Plan view of the Test One experimental compartment showing slice place section S1-S1 relative to furniture layout (to scale) and fire-monitoring sensor locations. Slice plane sections S2-S2 and S3-S3 are shown relative to external thermocouple sensors. The boxed region indicates the area corresponding to ceiling Heat Flux plots. The global coordinate system origin is also indicated.

The contour plots given in Figure 6 represent a slice plane (defined by a y-axis coordinate of 3021mm) that traverses the compartment from the window to the kitchen partition wall such that it cuts across the main area of pre- and early post-flashover fire spread. This slice plane is indicated as an S1-S1 section (encompassing thermocouple trees 1,5,7,10,13 and 16) in Figure 7 which also references the global origin from which the contour plot axes indicate distances in millimetres. The temperature transition during the flashover period is evident between Time Steps 2-3 (Figures 6b, 6c) by the change from a distinct localised fire to multiple spots of intense burning and high temperatures throughout the compartment, with the descent of the smoke layer. Although the bookcases and a computer station seem to be contributing significantly towards the temperature increase there is a shift towards greater temperature homogeneity seen in Time Step 4 (Figure 6d). This is further evident in Time Step 5 (Figure 6e), concurring with the reduction in standard deviation of mean compartment temperatures noted in Figure 5. Once the first window pane has broken, Time Step 6 (Figure 6f) highlights the marked increase in global compartment temperature as the partially-combusted fuel is consumed.

A collection of these temperature contour plots representing several slice planes throughout the compartment can provide a detailed indication of the 3-D spatial evolution of temperature throughout the development of the fire. These plots can be particularly useful for comparison with similar temperature slice plane files obtainable as output from several CFD modelling tools.

Heat Flux

Heat flux measurements have also been used to characterise the Test One fire. Spatial variation of heat flux may lead to varying severity of structural exposure to fire which will influence the behaviour of structural response, rendering heat flux an important fire characteristic for structural analysis.

Heat flux gauges located across the compartment ceiling (*cf.* Figure 7) and on the kitchen partition wall (*cf.* Chapter 2, annex Figure A1) were spaced such that they provided data representative of the global distribution of flux incident on those surfaces. Net incident heat flux contour plots were prepared for each key time step, providing a comparison of heat flux evolution as the fire developed.
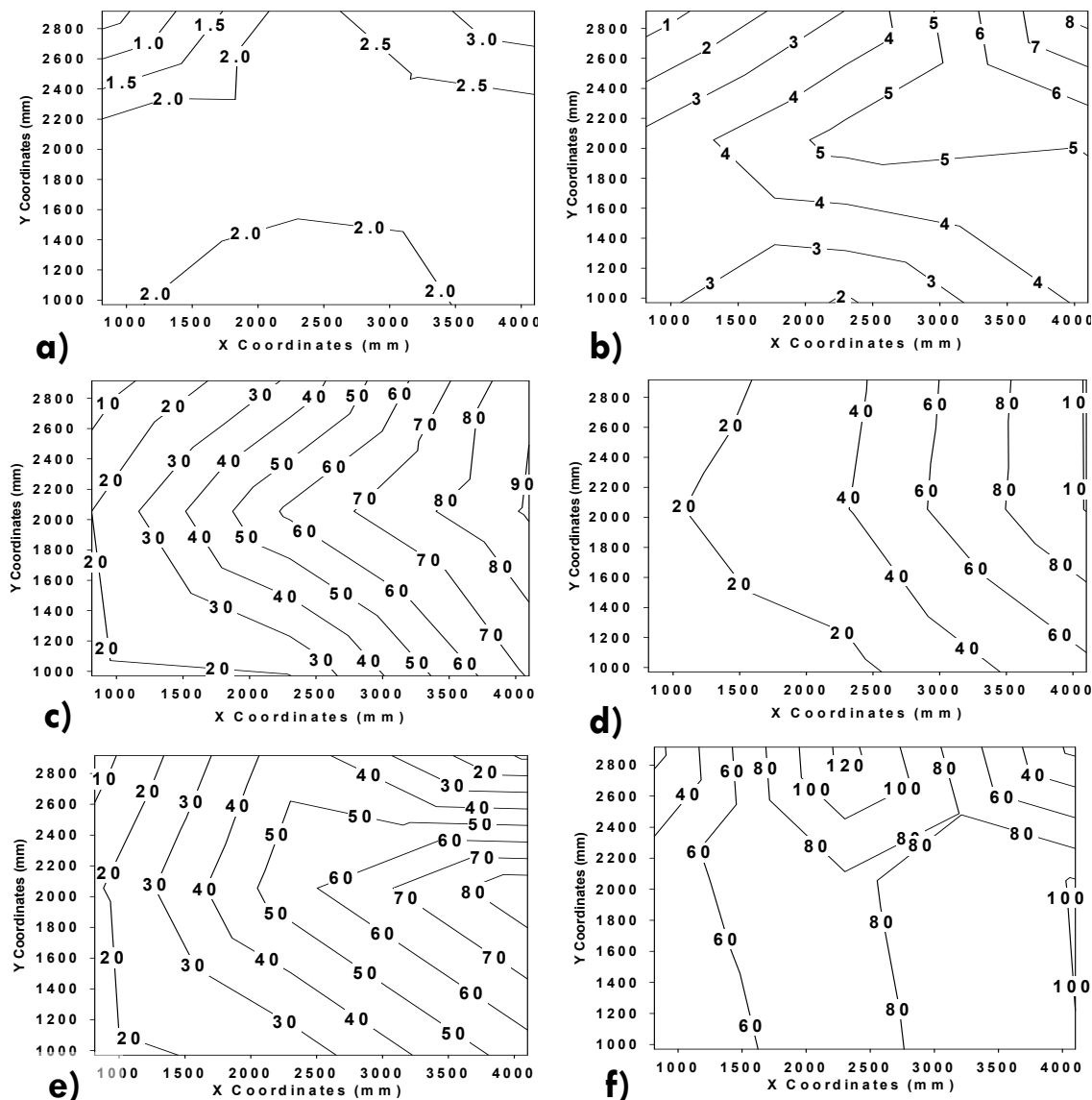
Figure 8. Contour plots of heat flux (in kW/m²) incident on the experimental compartment ceiling region indicated on Figure 7.
Axes values read distances from the global origin (*cf.* Figure 7). Plots appear in the Time Step chronological order, at times from ignition: a) 201s, b) 251s, c) 351s, d) 420s, e) 661s, and f) 901s.

Patterns of peak heat flux to the ceiling over time, shown in Figure 8, are seen to correlate to sharp rises in gas-phase temperature, particularly with the notable circa ten fold rise in heat flux to the ceiling between Time Steps 2-3 (Figures 8b, 8c), *just* pre- and post-flashover. Similarly, there is a notable increase in global heat flux incident on the ceiling between Time Steps 5-6 (Figures 8e, 8f), as average compartment temperature rises once ventilation conditions change. The contour plots also demonstrate a tendency for higher fluxes towards the back of the compartment, over the sofa and heavily fuel-loaded NE corner, particularly as the flaming fire develops between Time Steps 2 and 6 (Figures 8b-8f). This illustrates how regular compartment fires can lead to a varying gradient of insult to a single structural component (*i.e.* beams, floor slabs, etc.). Similar conclusions can be drawn from contour plots of heat flux incident on the kitchen partition wall.

Further analyses of post-flashover heat fluxes to the compartment ceiling and kitchen partition wall are discussed in detail in Chapter 7. Chapter 8 also provides an overview of the structural response, as a study of the structural-monitoring sensor data, such as the delayed heating of the concrete slab which to some extent is anticipated by the patterns of heat flux incident on the ceiling.

Heat Release Rate

Analysis of velocity probe data allows for an approximate quantification of the fire size in terms of the overall Heat Release Rate (HRR). This provides the essential parameter characterising the fire source.

Total Heat Release Rate was derived from bi-directional velocity probe data using the principle of oxygen depletion calorimetry described by Huggett (1980). Since no calorimeter or gas sampling measurements were available, the calculation has been based on the assumption that all oxygen (23% air, by mass) was consumed within the compartment, giving an upper bound estimate of HRR. Therefore, this study was only possible for the period when fire flows became significantly dominant over ambient flows, around the time of Time Step 2 and the HRR for the initial fire growth period shown in Figure 9 is only indicative of that expected. For the majority of the post-flashover period only the six probes located in the two compartment doorways were used for calculation of HRR, as the compartment window panes only broke towards the end of the observed post-flashover fire. Although the doorway velocity probe data was very localised and fluctuated considerably, together with a number of assumptions it allowed for an estimate of the magnitude of characteristic HRR throughout the fire.

Total gas mass inflow and outflow derived from the velocity probe data were found to be imbalanced, particularly in the early post-flashover period where there seems to be a deficit of mass inflow. There are a variety of possible reasons for this variation, namely the limited number of probes and the location of these probes. The lowermost probes were still 430mm and 460mm off the ground, which may not have accounted for the majority of the inflow area since the smoke layer had descended considerably post-flashover. Also, the local temperature values used to calculate the gas density surrounding probes in both doorways were those singly measured by thermocouples in tree 4, located

in between the two doors (*cf.* Figure 7). This tree was a horizontal distance of 250mm away from the probes in Door 2 and 930mm from those in Door 1 (negligible vertical discrepancy). This meant the same local gas density was assumed for probes at similar heights in both doorways, when in reality they were likely to be quite different due to ventilation relative to the flat geometry. An average of both mass inflow and outflow was used ensuring the balance of both. Assuming complete combustion of all oxygen, Huggett's formula was then used to estimate the Heat Release Rate from the mass flow data (Huggett 1980) seen in Figure 9.
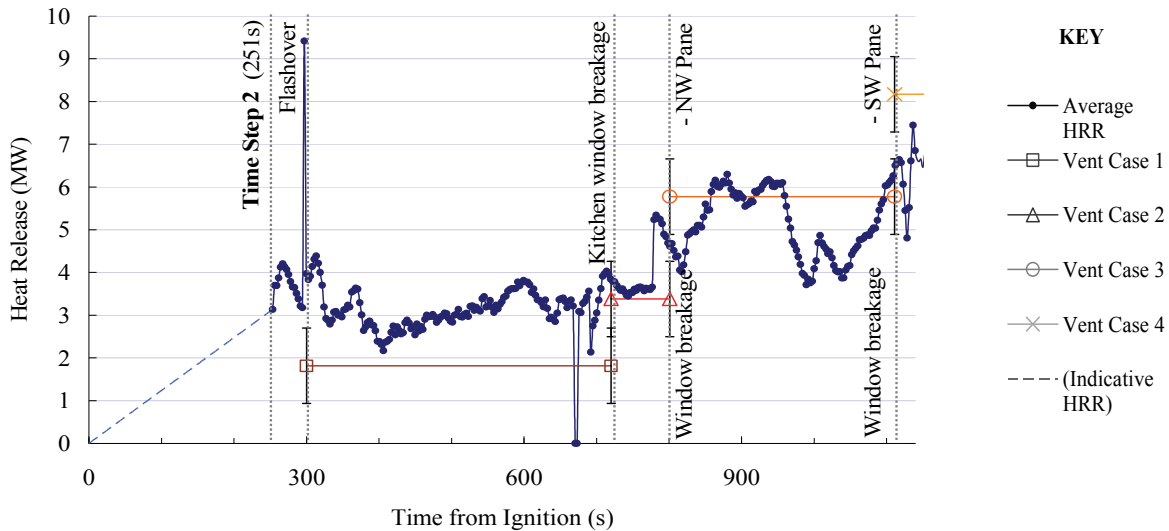
Figure 9. Heat release rate of the fire as estimated using the principle of oxygen depletion. Alternative simplified estimates using ventilation factors for the calculation of HRR are shown as Vent Cases corresponding to different ventilation change events. These include error bars and indicate good agreement with the HRR calculated from velocity probe data. Timing of some major events is represented by vertical dotted lines, as labelled.

Due to the number of assumptions involved in the assessment of HRR, a check was performed using estimated ventilation factors to compute mass inflow rates for different periods throughout the ventilation-controlled fire. Compartment ventilation factors were calculated for each ventilation condition, in the form of Vent Cases (Kawagoe 1963). Vent Case 1 assumed 30% of the kitchen window area was open and that 50% equivalent of the Flat Corridor area (height reduction) was open to simulate the initial ventilation conditions. Once the kitchen window shattered this was taken into account in the ventilation factor of Vent Case 2. Similarly, when the compartment NW window pane broke, this was integrated in the conditions for Vent Case 3. Final Vent Case 4 includes ventilation from both compartment window panes further to the kitchen window and initial conditions. Again, using Huggett's formula (Huggett 1980) and assuming complete combustion of oxygen to obtain basic HRR values, these cases are plotted and indicate

good agreement between both methods, illustrated in Figure 9. Laboratory tests, described in detail in Chapter 6, were conducted using calorimetry to determine the average Heat Release Rate of replica items of furnishings used in Test One. These were also used to verify the magnitude of values of the global HHR trend were within the expected range.

The overall Heat Release Rate trend corresponds to that of the average compartment temperature. The HRR is seen to grow from a quasi-steady state 3MW fire to a larger ~5MW fire around the time when the first compartment window breaks, accountable also for the distinct increase in average compartment temperatures between Time Steps 5 and 6 seen in Figure 5. Although this is a relatively crude measurement of HRR it provides a good indication of the order of magnitude of the fire size throughout Dalmarnock Fire Test One.

External Fire

Analysis of the external fire also contributes to the characterisation of Dalmarnock Fire Test One. Post-flashover some external flaming was observed once the compartment window shattered. Since this took place towards the later stages of the fire (after Time Step 5), a different time frame was used to compare external thermocouple and heat flux data collected, mostly within the final 5-6 min period of the fire. Nevertheless the compartment windows were not air-tight and it is worth analysing some data collected during the initial post-flashover stage where a limited amount of smoke was emanating from small gaps around the window frames. This allows for comparison of the change in external temperature and heat flux measured after the window broke and to quantify the significance of an external smoke plume as opposed to a flaming spill plume.

External thermocouple trees were arranged such that temperature contour plots could be used to map the three-dimensional variation of the external spill plume, in time. External thermocouple temperature measurements have not been corrected for radiation errors since application of the correction methodology in external flows requires a good knowledge of the local velocity fields (Welch *et al.* 2007). Despite the deployment of velocity probes in the main window opening there remains considerable uncertainty on the plume geometry due to the effect of other influences on the external flows which are hard to quantify. These include the direction and general intensity of the air movement past the building due to the wind and at a smaller scale, the significant turbulent fluctuations in these flows. The wind was observed to change in direction during the test (Figure 10) and had an effect on the amount of exhaust gases emerging from each external opening. Therefore external thermocouple measurements have been assumed to correspond directly to spill plume gas-phase temperature, for the purposes of this analysis.
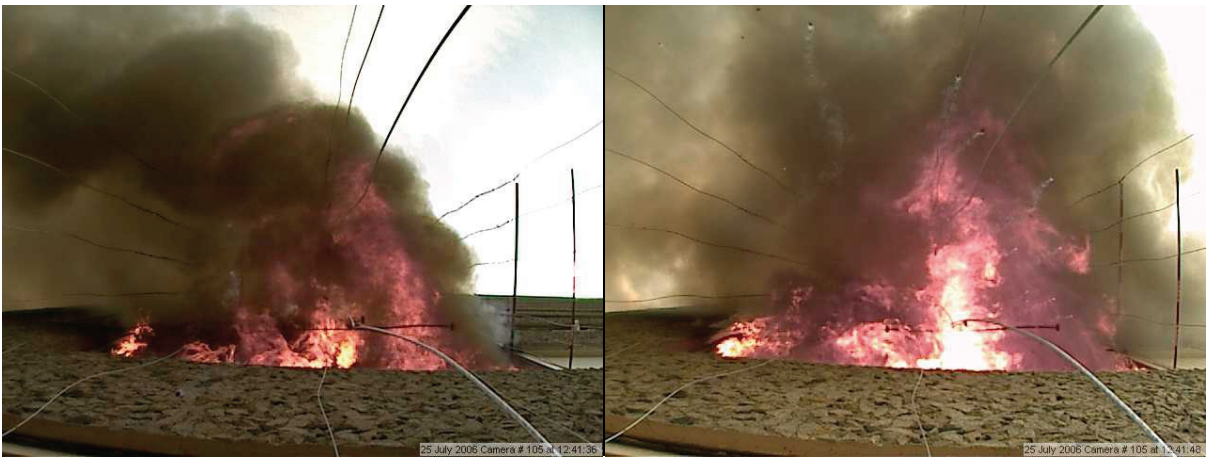
a)   b)

Figure 10. Camera footage taken at 3rd floor level, looking up at the external fire emanating from experimental compartment window. The spill plume images, taken 12 s apart, highlight the extent of change in local wind conditions from: a) a distinct North-facing wind (at 12:41:36), to b) barely noticeable wind (at 12:41:48).
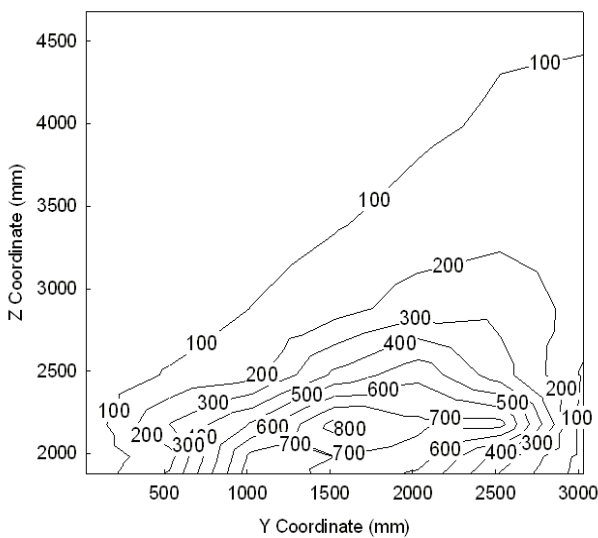
a)

Figure 11. External spill plume temperature contours (in °C) taken from sections a) S2–S2 (at 12:41:36) and b) S3–S3 (at 12:41:36), with axes values reading distances from the global origin (*cf.* Figure 7).
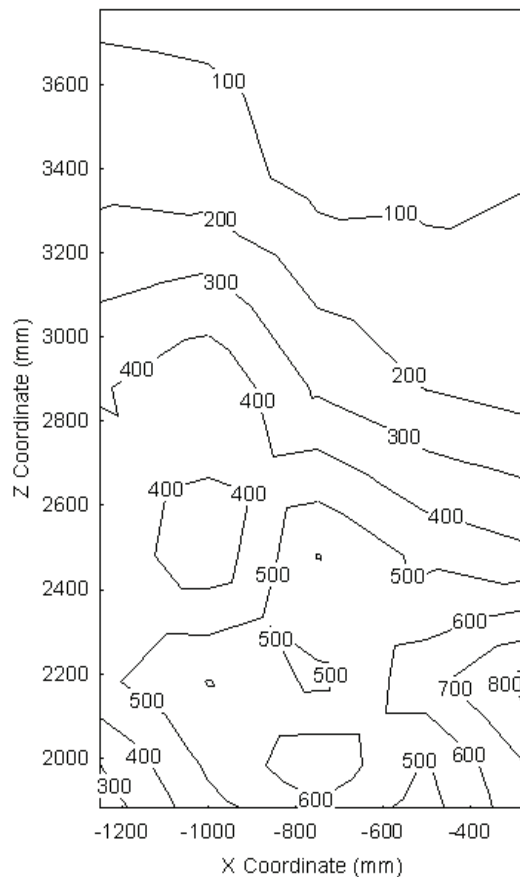
b)

Prior to window breakage maximum external temperatures recorded were of the order of ~230ºC, registered by thermocouples closest to the top ridge of the NW window pane, observed to be engulfed by smoke seeping through the window frame. The average of maximum temperatures recorded by each external thermocouple during this period however was still relatively low at ~60ºC. Following breakage of the first window pane most thermocouples registered a significant increase in temperature, particularly those in the NW half of the arrangement. Maximum external thermocouple temperatures registered were ~860ºC, with an average of ~400ºC including all thermocouples spanning up to the mid-height of the 5th floor window. The variation in temperature across the plume shown in the Figure 10a image can be seen in Figure 11. Temperature contour plots are such that section S2-S2 (Figure 11a) encompasses thermocouple trees E1-E7, parallel to the experimental compartment window (*cf.* Figure 7) and section S3-S3 (Figure 11b) encompasses thermocouple trees 4,9,12,15 and 18, perpendicular to the window down its centreline (*cf.* Figure 7). These plots show a large temperature gradient throughout the plume and can be use to determine the geometry of the external spill plume as it varies in time. Figure 11a shows temperature contours as viewed from the window, the plume outline indicated by the 100ºC contour highlighting the affect of the north-westerly wind on the plume, also observed in the Figure 10a image.

External heat flux sensors were arranged such that a general representation of the heat flux impingent on the façade could be used to analyse the fire insult to the external part of the structure. A set of 12 vertically aligned heat flux gauges provided the vertical variation in heat flux, centrally aligned from just above the 4th floor window to the top of the 5th floor window above. A set of four horizontal heat flux gauges (two either side of the vertical gauges) just above the experimental compartment window and an equivalent set across the mid-height of the 5th floor window above allowed for heat flux contour plots to encompass some of the horizontal distribution in incident flux.

Prior to the breaking of the window the maximum external incident heat flux recorded was of the order of 10.5kW/m^2, impinging on the area just above the compartment window sill. This coincided with the area of maximum external temperature recorded, where smoke was observed. After the initial window breakage the maximum incident heat flux observed is directly above the NW window pane, however once both panes break a maximum value of $\sim 60\text{kW/m}^2$ is recorded just above the centre of the window arrangement. This range of heat flux is expected given the $20\text{-}60\text{kW/m}^2$ internal heat flux to the experimental compartment ceiling in the vicinity of the window between Time Steps 5-6 (Figures 8e, 8f). There is a clear decrease in maximum heat flux to the façade further up from the compartment window, as would be expected. Although there is some horizontal variation in maximum heat flux to the façade, in that heat flux decreases with distance from the central area directly above the windows, this trend is not as evident at 5th floor level as it is directly above the compartment opening. Although local wind variation appears to have affected the angle of the spill plume throughout the fire, evident from both sensor data and camera footage (Figure 10), once both window panes break the fire seems to exert the most sustained and severe insult to the façade centrally above the window.

These features of the external fire, together with visual information, can be instructive of characteristics of the internal fire. Characteristics of the external fire are also vital for research into the importance of the spill plume insult to the external façade and the impact this may have on the global behaviour of the structure in fire.

Summary and Exploitation

Test One was a full-scale fire experiment that successfully developed into an unrestrained post-flashover fire. The high density and broad range of sensors employed allowed for a complete characterisation of all aspects of the fire, including the pre- and post-flashover phases, as well as the development of the internal and external fires.

The realistic fuel distribution provided conditions that favour repeatability and together with the sensor density has provided data that is ideal for field model validation, as further discussed in Chapters 10 and 11. The complete characterisation of this test has allowed for comparison with a similar analysis of Test Two, which to some extent enabled an evaluation of the repeatability of the test scenario further discussed in Chapter 4. This characterisation has also allowed for the subsequent analysis of structural behaviour and that of a series of other demonstrations not directly associated with the fire development. Consequently, the results of such analyses can be implemented in the validation of a range of other related modelling tools.

Acknowledgements

References

Huggett, C. (1980), Estimation of Rate of Heat Release by Means of Oxygen Consumption Measurements, Fire and Materials, 4, p.61-65.

Jin, T. (2002), Visibility and Human Behaviour in Fire & Smoke, Chapter 4, The SFPE Handbook of Fire Protection Engineering, 3rd Edition, National Fire Protection Association, Massachusetts, U.S.A., p. 2-43.

Kawagoe, K. and Sekine, T. (1963), Estimation of fire temperature-time curve in rooms. BRI Occasional Report 11, Building Research Institute, Tokyo.

McCaffrey, B.J. & Heskestad G. (1979), A Robust Bidirectional Low-Velocity Probe for Flame and Fire Application, Combustion and Flame 26, 125-127.

Mulholland, G.W. (2002), Smoke Production and Properties, The SFPE Handbook of Fire Protection Engineering, 3rd Edition, National Fire Protection Association, Massachusetts, U.S.A., p.2-263, 2-265.

Welch, S., Jowsey, A., Deeny, S., Morgan, R., Torero, J.L. (2007), BRE Large Compartment Fire Tests – Characterising Post-Flashover Fires for Model Validation, Fire Safety Journal, in press.

The opinions expressed in this volume are those of the named authors of each of the chapters and may not represent the opinions of the editors, the School of Engineering and Electronics or the University of Edinburgh.

When citing chapters from this volume, the following reference style should be used:

Authors, Chapter no., Title, The Dalmarnock Fire Tests: Experiments and Modelling, Edited by G. Rein, C. Abecassis Empis and R. Carvel, Published by the School of Engineering and Electronics, University of Edinburgh, 2007. ISBN 978-0-9557497-0-4

The contents of this book and much of the other published output from the BRE Centre for Fire Safety Engineering can be downloaded from the Edinburgh Research Archive:

http://www.era.lib.ed.ac.uk/handle/1842/1152

Produced as part of the FIRESEAT symposium series:

http://www.see.ed.ac.uk/FIRESEAT/